J. Phys. D: Appl. Phys. **42** (2009) 015408 (5pp) doi:10.1088/0022-3727/42/1/015408

X-ray photoelectron spectroscopy of Er^{3+}-activated SiO_2–HfO_2 glass-ceramic waveguides

L Minati[1,3], G Speranza[1], V Micheli[1], M Ferrari[2] and Y Jestin[2]

[1] FBK via Sommarive 18, Povo, 38100 Trento, Italy
[2] CNR-IFN, Istituto di Fotonica e Nanotecnologie, CSMFO Lab., Via alla Cascata, 56/C, Povo, 38100 Trento, Italy

E-mail: luminati@fbk.eu

Received 23 September 2008
Published 10 December 2008
Online at stacks.iop.org/JPhysD/42/015408

Abstract

xHfO$_2$–(100 − x) SiO$_2$ (x = 10, 20, 30 mol%) glass-ceramic planar waveguides doped with 0.3 mol% Er^{3+} ions, prepared by the sol–gel route and heat treated at 1000 °C to nucleate HfO_2 crystals, were analysed by x-ray photoelectron spectroscopy, x-ray diffraction, high resolution transmission electron microscopy and photoluminescence spectroscopy. Formation of tetragonal HfO_2 nanocrystals has been evidenced in all the samples. Spectroscopic parameters concerning the $^4I_{13/2}$ metastable state of Er^{3+}ion are revisited as a function of XPS analysis.

1. Introduction

Rare-earth-activated glass-ceramics (GCs), where a glass host is loaded with a crystalline phase containing the active ions, are emerging materials in photonics because they combine the advantages of optical glasses with crystal-like spectroscopic characteristics [1, 2]. During the last few years our group has carried out research in this field, in particular, on sol–gel-derived Er^{3+}-activated HfO_2-based GCs [2–5]. We demonstrated that using a suitable top-down [5, 7] and bottom-up technique [2] it is possible to fabricate Er^{3+}-activated planar waveguide SiO_2–HfO_2 GCs [2, 5]. From the optical and spectroscopic points of view this research activity has evidenced that (i) silica–hafnia GCs allow us to achieve an attenuation coefficient as low as 0.3 dB cm^{-1} at 1542 nm, and (ii) the HfO_2 crystalline phase can efficiently enhance the spectroscopic properties of erbium ions [2, 3, 5, 7]. Regarding the structural properties of this kind of GCs only a preliminary work using x-ray absorption fine structure (EXAFS) has been published [4]. Particular attention has been paid to obtaining chemical and structural information about the parent amorphous silica–hafnia waveguides [4, 6]. With this aim x-ray photoelectron spectroscopy (XPS) measurements performed on the amorphous waveguides as a function of hafnia content allowed us to identify both structural changes and the critical HfO_2 abundance at which the phase separation occurs [6]. In particular, we have demonstrated that for HfO_2 content higher than 30 mol% phase separation occurs [6]. On the basis of these results waveguiding GCs were fabricated by the top–down technique starting from parent $(100 - x)SiO_2$–xHfO$_2$ amorphous waveguides with $x \leqslant 30$. Their spectroscopic and optical assessments were reported in [5].

Here we employ the XPS technique to investigate the structure of these sol–gel-derived GC waveguides of composition $(100 - x)SiO_2$–xHfO$_2$ (x = 10, 20, 30) and give a correlation with the spectroscopic properties concerning the $^4I_{13/2}$ metastable state of Er^{3+} ions reported in [5].

2. Experimental

Er^{3+}-activated planar waveguide SiO_2–HfO_2 GCs are the same used for the assessment of their optical and spectroscopic properties reported in [5]. Without going into details, the parent waveguides were amorphous waveguides of composition $(100 - x)SiO_2$–xHfO$_2$ (x = 10, 20, 30) activated by 0.3 mol% Er^{3+} ions, prepared by the sol–gel method. Er^{3+}-activated SiO_2–HfO_2 films were deposited on v-SiO_2 substrates by the dip coating process. Final films, resulting from 30 to 35 coatings, were stabilized by a last treatment in air at 900 °C (table 1). As a result of this procedure, transparent,

[3] Author to whom any correspondence should be addressed.

 © 2009 IOP Publishing Ltd Printed in the UK

amorphous and crack-free waveguides were obtained. In order to nucleate nanocrystals inside the parent planar waveguide an additional heat treatment was performed at 1000 °C for 30 min [5].

XP spectra were acquired using a 200 mm Scienta (Gammadata—Uppsala) hemispherical analyzer and monochromatized Al K_α radiation. The vacuum was in the range of 10^{-8} Pa. For each sample a wide scan, 0–1200 eV, was performed to detect the chemical elements together with possible contaminations. Core lines were acquired using a pass energy of 150 eV. The value of 284.6 eV of the carbon core line due to contaminants was used as a reference to determine the correct binding energy (BE) values of the other chemical elements. In this condition the energy resolution of the analyzer at the Fermi edge is about 0.4 eV. An Italstructures APD 2000 diffractometer with a Cu $K_{\alpha 1}$ radiation and a NaI(Tl) crystal as detector was used to obtain the x-ray diffraction (XRD) patterns with a Bragg–Brentano geometry.

Specimens for high resolution transmission electron microscopy (HRTEM) measurements were prepared by scraping off thin films in absolute ethanol using a diamond knife. A drop of the suspension was deposited and dried onto a carbon coated copper grid. HRTEM studies of the scraped samples were performed in a 200 kV JEOL 2010 transmission electron microscope.

3. Results and discussion

3.1. XPS analysis

In figure 1(*a*) the Si 2p core lines of pure silica reference and those of the samples at different HfO_2 contents are reported.

Table 1. Compositions and heat treatment duration of the erbium activated $xHfO_2$-$(100-x)SiO_2$ GC planar waveguides [5].

Sample label	$SiO_2 : HfO_2$ molar ratio	Er^{3+} mol%	Total annealing time at 900 °C	Annealing time at 1000 °C
SH10	90 : 10	0.3	30 h	30 min
SH20	80 : 20	0.3	210 min	30 min
SH30	70 : 30	0.3	5 min	30 min

The spectra are normalized to a common intensity value. The position of the peaks shows that all the silicon atoms in the samples are in the IV oxidation state [6]. An increase in the hafnium concentration leads to a shift in the Si 2p BE. The origin of the shift is linked to the lower electronegativity of hafnium with respect to silicon. This causes a charge transfer to the nearest Si atoms, in order to equalize the total electronegativity of the material [8]. On the other hand, when the negative partial charge of a given component element increases, its XPS BE lowers [9]. This enables one to discriminate the pure SiO_2 from hafnium silicate ($HfSiO_n$ regions) present in the sample. From the spectral point of view this behaviour is mirrored by the appearance of a feature placed on the low BE side of the Si 2p line which causes a sensible broadening [6] (see figure 1(*a*)).

After linear background subtraction the Si 2p core lines were fitted with two Gaussian components. One peak at around 103.4 eV refers to the SiO_2-like bonds, while the second peak at around 102.4 eV is associated with the silicon atoms in hafnium silicate.

In figure 1(*b*) we report the Hf 4f core lines from pure HfO_2 and from the SiO_2–HfO_2 GC waveguides. The increasing Hf content induces a peak broadening on the high BE side. This reflects the presence of two components: the first related to Hf–O–Si bonds and the second to HfO_2 as a result of the phase separation process. As for Si 2p, the Hf $4f_{7/2}$ (Hf $4f_{5/2}$) lines were also fitted with two components: one at ∼17.6 eV (19.27 eV) representative of hafnium silicate and one at ∼17.0 eV (18.68 eV) associated with HfO_2.

Figure 2(*a*) shows the O1s core lines of the three GCs normalized at the same height. The changes in the line shapes due to the variation of the relative amounts of hafnium silicate and HfO_2 are clearly visible. In figure 2(*b*) the fit of the SH30 GC is reported. Three peaks are necessary to describe the O 1s curve. The peak at ∼532.6 eV corresponds to SiO_2 while the one at ∼530.4 eV is relative to HfO_2. The intermediate component at ∼531.5 eV refers to oxygen in hafnium silicate in agreement with the literature [10]. The results of the fits are reported in table 2.

The incertitude of the values is ∼3%.

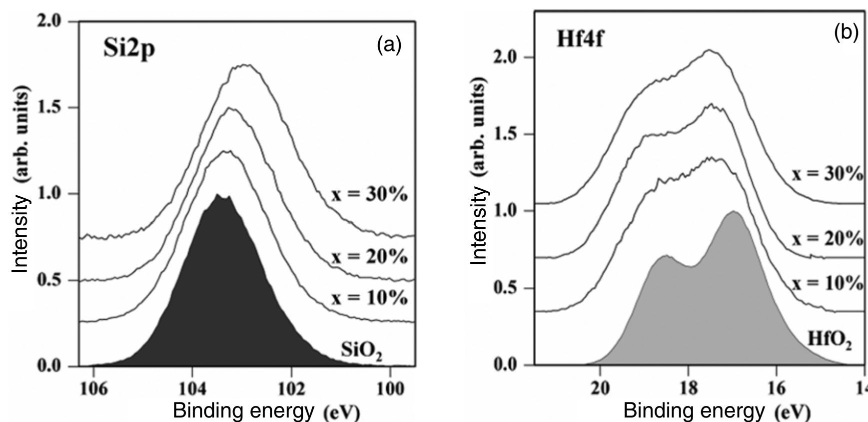

Figure 1. (*a*) Si 2p core line of SiO_2–HfO_2 GC waveguides, with different HfO_2 molar concentrations, normalized at the same height; (*b*) Hf 4f core line of SiO_2–HfO_2 GC waveguides, with different HfO_2 molar concentrations normalized at the same height. Dark and grey spectra represent the pure SiO_2 and HFO_2 references, respectively.

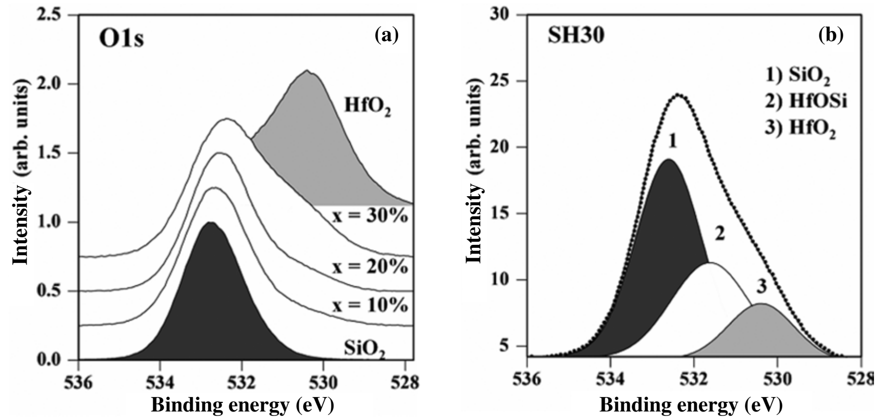

Figure 2. (*a*) O 1s core line of SiO_2–HfO_2 GC waveguides, with different HfO_2 molar concentrations, normalized at the same height; (*b*) fit of the O 1s line of SH30 GC. Dark and grey spectra represent the pure SiO_2 and HFO_2 references, respectively.

Table 2. XPS percent atomic abundances measured on the SiO_2–HfO_2 GC waveguides. Incertitude is 3%.

Element	Bond	SH10	SH20	SH30
Si%	SiO_2	23.34	24.18	16.09
	Hf–O–Si	2.48	5.53	11.39
Hf%	Hf–O–Si	2.11	3.27	6.1
	HfO_2	1.25	2.73	4.26
	SiO_2	56.52	48.97	32.56
O%	Hf–O–Si	8.72	9.56	22.11
	HfO_2	2.52	5.76	8.40

The XPS spectra demonstrate that hafnium is present in two chemical forms: hafnium silicate homogeneously distributed in the amorphous SiO_2 and HfO_2 crystals. In addition, XPS analysis indicates that at 1000 °C the degree of crystallization of HfO_2 is low. In fact, the hafnium mobility at this temperature is too low to allow a migration through the silica network leading to a total HfO_2 crystallization. As evidenced in table 2 in all the GCs the amount of Hf in amorphous phase is higher than the concentration of Hf in the crystalline phase. This result suggests that by using a suitable thermal treatment it is possible to tailor both size and volume fraction of HfO_2 nanocrystals without creating large scale inhomogeneities in the glass composition that would cause an increase in the propagation losses in the waveguides [2, 7].

In conclusion, from the XPS analysis we can estimate the relative amount of HfO_2 nanocrystals in the GCs. A correlation between these data and the optical spectroscopic response will be discussed later on.

3.2. XRD analysis

The XRD patterns of GCs SH10, SH20 and SH30 shown in figure 3 are assigned to HfO_2 in the tetragonal crystalline phase [11].

The spectral features of the SH10 sample are broader with respect to the other two samples. This corresponds to smaller particles whose volume-weighted mean dimensions can be estimated using the Scherrer law [12]:

$$\langle D\rangle_{\mathrm{vol}} = K\lambda_{K\alpha 1}/(B_{2\theta}\cos\theta), \qquad (1)$$

where $\langle D\rangle_{\mathrm{vol}}$ is the volume-weighted mean particle size, K is a constant that depends on the acquisition geometry and on the plane index (∼0.9 in our case), $\lambda(K_{\alpha 1})$ is the x-ray wavelength (1.540 56 Å for Cu $K_{\alpha 1}$ radiation) and $B_{2\theta}$ is the peak broadening where the angle θ corresponds to the peak maximum.

We chose the peak at about $2\theta = 50°$ for the analysis because it is well resolved and it has a good intensity to perform a precise analysis. The results of the fit are shown in table 3. The SH20 and SH30 GCs have HfO_2 nanocrystals with a mean size of about 5 nm. In the case of SH10 GC the dimension of nanocrystals is estimated to be about 3 nm as expected on the basis of the lower Hf concentration.

Although XRD does not provide information about the decomposition mechanism that leads to the formation of the nanocrystals, the small dimensions of the clusters and their crystalline phase point to the occurrence of spinodal decomposition [13].

The tetragonal crystalline structure is known to be metastable. The presence of this phase instead of the more stable monoclinic phase may be explained on the thermodynamical basis. In fact, due to the high volumetric strain involved, the transformation from tetragonal to monoclinic structure occurs at a rather low speed. This process is then favourable in systems in which nucleation and growth are separate mechanisms expected to create larger grain size [14].

3.3. TEM analysis

The TEM image of SH30 GC reported in figure 4 shows a phase separation in amorphous SiO_2 domains (light regions) and HfO_2 rich regions (dark regions). The high magnification inset clearly evidences the presence of semi-spherical crystals grown in the dark regions, which are identified as HfO_2 nanoclusters of ∼5 nm (in our experimental conditions formation of crystalline hafnon $HfSiO_4$ is kinetically excluded [15]). The energy dispersive x-ray analysis confirmed that the nanocrystals are composed of Hf oxide and that the surrounding amorphous matrix is constituted by silica. As a matter of fact, the distance between two adjacent lattice

Figure 3. XRD patterns of the SH10, SH20 and SH30 GCs.

Table 3. XRD pattern analysis results of $xHfO_2$-$(100 - x)SiO_2$ planar waveguides GC.

XRD	SH10	SH20	SH30
2θ (°)	50.12	50.48	50.67
FWHM (°)	4.62	2.96	2.80
$\langle D \rangle_{vol}$ (nm)	3.5 ± 1	5.2 ± 1	5.8 ± 1

fringes is ~0.354 nm in agreement with the interplanar distance that in the (1 1 1) bulk tetragonal HfO_2 crystal is about 0.360 nm [11].

The presence of well-defined dark and light regions with lengthened shape demonstrates the presence of spinodal decomposition. We can confirm that the crystallization of hafnia is confined to the HfO_2 rich zones. This process depends on the annealing time, on the temperature and on the HfO_2 content in the samples. These parameters allow a control of the dimensions and of the distribution of the nanocrystals. Ushakov *et al* [16] have calculated the crystallization enthalpies for SiO_2–HfO_2 systems with different Hf contents. Their differential scanning calorimetry analysis evidenced a decrease in the HfO_2 crystallization enthalpies with an increase in the crystalline size. This result is caused by the high interface energy (0.25 J m^{-2}) between HfO_2 crystals and amorphous SiO_2. As a consequence, the formation of big nanocrystals is favourable with respect to small nanocrystals and tetragonal phase is energetically favourable with respect to the monoclinic one.

Then, once the HfO_2 domains are formed, further applications of annealing lead to an increase in spinodal decomposition rather than a regression of the phase separation. Moreover, the experiments demonstrate that a short thermal treatment at 1000 °C is able to induce crystallization of the hafnia domains. The nucleation of the crystals in the tetragonal phase starts probably at the centre of the HfO_2 rich phases (dark zone) and proceeds towards the SiO_2 interface. The

Figure 4. TEM image obtained on SH30 waveguide GC. The inset shows high magnification image.

application of a fast thermal annealing induces the formation of HfO_2 crystals whose nanometric dimensions are determined by the coarsening of the separated textures [17].

3.4. Er^{3+} spectroscopic properties

The PL spectra for the GC waveguides SH10, SH20 and SH30 in the region of the $^4I_{13/2} \rightarrow {}^4I_{15/2}$ transition of Er^{3+} ions, obtained upon excitation at 514.5 nm, are reported in [5]. The presence of HfO_2 nanocrystals, directly linked to the hafnia content, is reflected by a change in the shape and bandwidth of the PL spectra with respect to those usually observed in the amorphous silica–hafnia system [17]. In particular, (i) GC PL spectra show well-resolved Stark components typical of Er^{3+} emission in a crystalline-like environment, (ii) the $^4I_{13/2} \rightarrow {}^4I_{15/2}$ spectral bandwidth measured at 3 dB from the

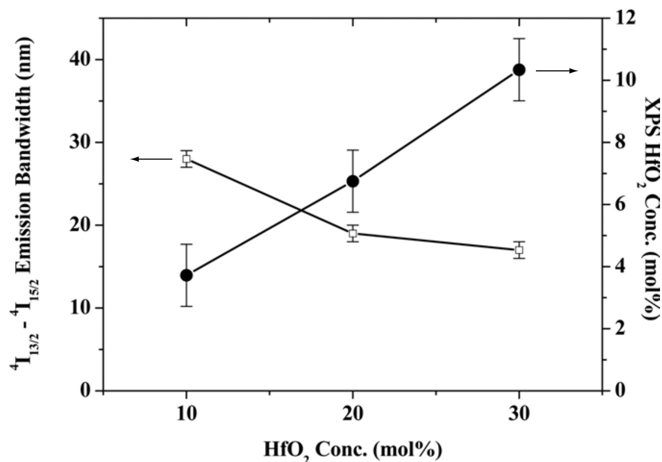

Figure 5. XPS crystalline HfO_2 concentration (right) and bandwidth of the of the $^4I_{13/2} \rightarrow {}^4I_{15/2}$ emission of Er^{3+} ions (left) for the SH10, SH20 and SH30 GC waveguides, as a function of the HfO_2 molar concentration.

maximum of the intensity are 28±1 nm, 19±1 nm, 17±1 nm for SH10, SH20, SH30 GCs, respectively, and (iii) the $^4I_{13/2}$ lifetime decreases from 9.0 to 8.7 and to 7.2, as the HfO_2 content increases from 10% to 20% and to 30% [5]. Note that the bandwidth of the parent planar amorphous waveguides is 50 ± 2 nm, due to the inhomogeneous broadening, for all the parent samples, and that the $^4I_{13/2}$ radiative lifetime is 7.1 ± 0.5 ms, 6.5 ± 0.5 ms and 5.9 ± 0.5 ms for x = 10, 20, 30, respectively [5, 18, 19].

Figure 5 reports the XPS concentrations of HfO_2 nanocrystals (right axis) and the $^4I_{13/2} \rightarrow {}^4I_{15/2}$ PL bandwidth (left axis) as a function of the HfO_2 content in the GCs. As expected, there is a linear correlation between the hafnia content and the relative abundance of HfO_2 nanocrystals and the narrowing of the $^4I_{13/2} \rightarrow {}^4I_{15/2}$ bandwidth is directly related to the number of HfO_2 crystallites in the samples.

Looking at the main differences between amorphous and GC waveguides, the spectroscopic behaviour is consistent with a change in the local environment around the erbium ions due to the formation of HfO_2 nanocrystals. As the Er^{3+} local environment becomes ordered, it limits the inhomogeneous broadening typical of glassy environment and, therefore, the bandwidth narrows. The increase in the lifetime in GCs with respect to the parent amorphous waveguides is explained by the fact that the crystalline environment induces the shortening of the non-radiative processes as well as a reduction in the luminescence quenching as discussed in [1, 5, 7].

As far as the GC systems are concerned, XPS results of figures 2(*a*) and (*b*) and table 2 show that the fraction of nanocrystals increases with the hafnium content, as expected, enhancing the probability of Er^{3+} ions embedding in the HfO_2 nanocrystals [4]. Spectroscopic parameters well fit this layout. The higher the hafnia content, the higher is the effect on the Er^{3+} spectroscopic properties due to the crystalline-like environment, i.e. significant narrowing of the emission bandwidth as well as lifetime lengthening is observed.

4. Conclusions

In this work we investigated sol–gel-derived GC waveguides of composition $(100 - x)SiO_2$–$xHfO_2$ (x = 10, 20, 30). XPS analysis shows the presence of two Hf states in all the samples: hafnium silicate-like and hafnium oxide. For all the samples the abundance of both these chemical states was estimated from core line analysis. XRD and TEM analyses have demonstrated the formation of tetragonal HfO_2 nanocrystals in all the samples with nanocrystal dimensions of about 3–5 nm depending on the HfO_2 content. TEM investigation on the SH30 sample has evidenced the presence of local composition fluctuation between SiO_2 and HfO_2 rich phase regions, indicative of spinodal decomposition. Hafnia nanocrystals are responsible for the narrowing of the spectral bandwidth of the $^4I_{13/2} \rightarrow {}^4I_{15/2}$ transition of Er^{3+} ions and of the lifetime lengthening with respect to the amorphous parent waveguides.

The combination of all these analytical techniques enabled us to unambiguously describe the mechanisms underlying the formation of nanostructures in SiO_2–HfO_2 waveguides and their chemical, structural and optical properties. Further work remains to exploit the spinodal decomposition process in Er^{3+}-activated GC waveguides.

References

[1] Mortier M 2002 *Phil. Mag.* B **82** 745
[2] Jestin Y, Armellini C, Chiasera A, Chiappini A, Ferrari M, Moser E and Retoux R 2007 *Appl. Phys. Lett.* **91** 071909-1
[3] Armellini C, Chiappini A, Chiasera A, Ferrari M, Jestin Y, Mortier M, Moser E, Retoux R and Righini G C 2007 *J. Nanomater.* **ID** 84745
[4] Afifi N D, Dalba G, Rocca F and Ferrari M 2007 *Phys. Chem. Glass.* **48** 229
[5] Jestin Y *et al* 2007 *J. Non-Cryst. Solids* **353** 494
[6] Minati L, Speranza G, Jestin Y and Ferrari M 2007 *J. Non-Cryst. Solids* **353** 502
[7] Jestin Y 2006 *SPIE Proc.* **6183** 438
[8] Sanderson R T 1971 *Chemical Bonds and Bond Energy* (New York: Academic)
[9] Briggs D and Grant J 2003 *Surface Analysis by Auger and X-Ray Photoelectron Spectroscopy* (Chichester, UK: IM Publication)
[10] Guittet M J, Crocombette J P and Gautier-Soyer M 2001 *Phys. Rev.* B **63** 125117
[11] International Centre for Diffraction Data Database (ICDD), http://www.icdd.com
[12] Warren B E 1996 *X-Ray Diffraction* (Reading, MA: Addison-Wesley)
[13] Kim H and McIntyre P C 2002 *J. Appl. Phys.* **92** 5094
[14] Ramanathan S, McIntyre P C, Luning J, Lysaght P S, Yang Y, Chen Z and Stemmerd S 2003 *J. Electrochem. Soc.* **150** F173
[15] Stemmer S, Chen Z, Levi C, Lysaght P S, Foran B, Gisby J A and Taylor J R 2003 *Japan. J. Appl. Phys., Part 1* **42** 3593
[16] Ushakov S V *et al* 2004 *Phys. Status Solidi* b **241** 2268
[17] Gaudon A, Dauger A, Lecomte A, Soulestin B and Guinebretère R 2005 *J. Eur. Ceram. Soc.* **25** 283
[18] Gonçalves R R, Carturan G, Zampedri L, Ferrari M, Montagna M, Righini G C, Pelli S, Ribeiro S J L and Messaddeq Y 2004 *Opt. Mater.* **25** 131
[19] Zampedri L *et al* 2004 *J. Non-Cryst. Solids* **345–346** 580